iScience

Article

Ltc1 localization by EMC regulates cell membrane fluidity to facilitate membrane protein biogenesis

Graphical abstract

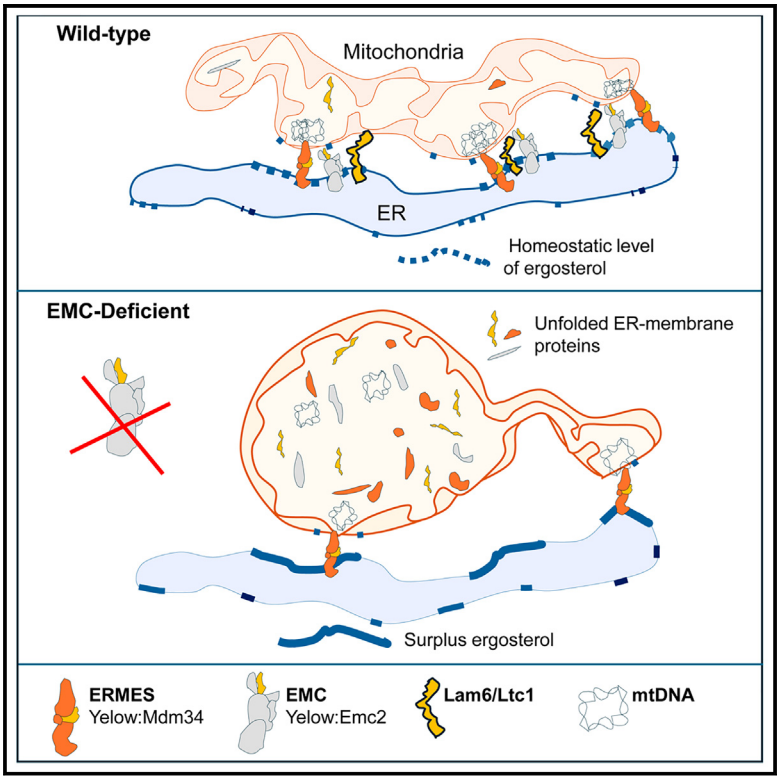

Highlights

- Lam6/Ltc1 requires EMC for proper localization at ER-mitochondria contact sites
- EMC-driven biogenesis of Lam6/Ltc1 is involved in membrane fluidity homeostasis
- EMC-deficient cells accumulate unfolded proteins in the mitochondrial matrix
- Cell membrane fluidization alleviates UPR of EMC-deficient cells

Authors

Modesto Berraquero, Víctor A. Tallada, Juan Jimenez

Correspondence

valvtal@upo.es (V.A.T.), jjimmar@upo.es (J.J.)

In brief

Biochemistry; Molecular biology; Cell biology

Berraquero et al., 2025, iScience *28*, 112096
March 21, 2025
https://doi.org/10.1016/j.isci.2025.112096

CellPress

iScience

CellPress
OPEN ACCESS

Article

Ltc1 localization by EMC regulates cell membrane fluidity to facilitate membrane protein biogenesis

Modesto Berraquero,[1] Víctor A. Tallada,[1,*] and Juan Jimenez[1,2,*]
[1]Centro Andaluz de Biología del Desarrollo, Universidad Pablo de Olavide/Consejo Superior de Investigaciones Científicas, Carretera de Utrera Km1, 41013 Seville, Spain
[2]Lead contact
*Correspondence: valvtal@upo.es (V.A.T.), jjimmar@upo.es (J.J.)
https://doi.org/10.1016/j.isci.2025.112096

SUMMARY

The EMC complex, a highly conserved transmembrane chaperone in the endoplasmic reticulum (ER), has been associated in humans with sterol homeostasis and a myriad of different cellular activities, rendering the mechanism of EMC functionality enigmatic. Using fission yeast, we demonstrate that the EMC complex facilitates the biogenesis of the sterol transfer protein Lam6/Ltc1 at ER-plasma membrane and ER-mitochondria contact sites. Cells that lose EMC function sequester unfolded Lam6/Ltc1 and other proteins at the mitochondrial matrix, leading to surplus ergosterol, cold-sensitive growth, and mitochondrial dysfunctions. Remarkably, inhibition of ergosterol biosynthesis, but also fluidization of cell membranes to counteract their rigidizing effects, reduce the ER-unfolded protein response and rescue growth and mitochondrial defects in EMC-deficient cells. These results suggest that EMC-assisted biogenesis of Lam6/Ltc1 may provide, through ergosterol homeostasis, optimal membrane fluidity to facilitate biogenesis of other ER-membrane proteins.

INTRODUCTION

The endoplasmic reticulum (ER) is a vast multifactorial membrane system of eukaryotic cells, the main site for lipid and carbohydrate biosynthesis, as well as for the folding, assembly, modification, and transport of secreted and integrated membrane proteins.[1,2] It is known to house many protein complexes that aid its function, including the conserved ER membrane protein complex (EMC).[3]

The EMC was first described in the budding yeast *Saccharomyces cerevisiae* as a complex composed of six proteins with similar genetic interaction patterns.[1] The structural integrity of the EMC depends on 'core subunits' EMC1, EMC2, EMC3, EMC5, and EMC6, which are essential for both assembly and function of the complex.[4–6] Two other membrane proteins, EMC7 and EMC10, also copurify with this complex to yield a mature eight-subunits complex.[7] An MS-based mapping of the ER-associated degradation (ERAD) interaction network not only confirmed the EMC orthologous in mammals but also identified EMC8 and EMC9, two metazoan-specific subunits.[8]

Biogenesis of membrane proteins at the ER requires insertion of proteins with specific topologies into lipid bilayers to carry out their functions.[1,4] The EMC assists many of them by promoting folding and insertion of their atypical and sub-optimal transmembrane domains (TMDs). Therefore, the EMC can function at the ER both co-translationally as a chaperone for folding TMD-containing proteins and post-translationally as an insertase for tail-anchored proteins.[9]

Notably, EMC complex dysfunction induces ER stress and changes/alterations to lipid transport and homeostasis, and organelle tethering among others.[3] Unraveling the primary relationship between EMC and the multifaceted cellular consequences of altering its client proteins remains a formidable challenge.

The fission yeast *Schizosaccharomyces pombe* is an important single-cell model organism widely used to study various aspects of eukaryotic cellular and molecular biology. In a genome-wide search for genes causing overexpression-mediated cell-cycle arrest in *S. pombe* cells ("*oca*" genes), we previously identified the *oca3* gene,[10] which encodes the putative EMC2 orthologous in vertebrates (Pombase: ID SPBC15C4.01c).[11] By analyzing the consequences of Oca3/Emc2 depletion, here we asked for the cellular and molecular mechanisms connecting EMC and the pleiotropic phenotypes observed in EMC dysfunctional *S. pombe* cells. Our results uncover that membrane fluidity homeostasis regulated by EMC is at the root of these cell defects.

RESULTS

Oca3 encodes the fission yeast ortholog to the metazoan EMC2

Sequence similarity predicts that the *oca3* gene encodes the putative fission yeast ortholog for the EMC2 subunit of the eukaryotic EMC complex.[12] To experimentally support this prediction, the encoded Oca3 protein was tagged with mCherry and expressed from its native locus in *S. pombe* cells co-expressing

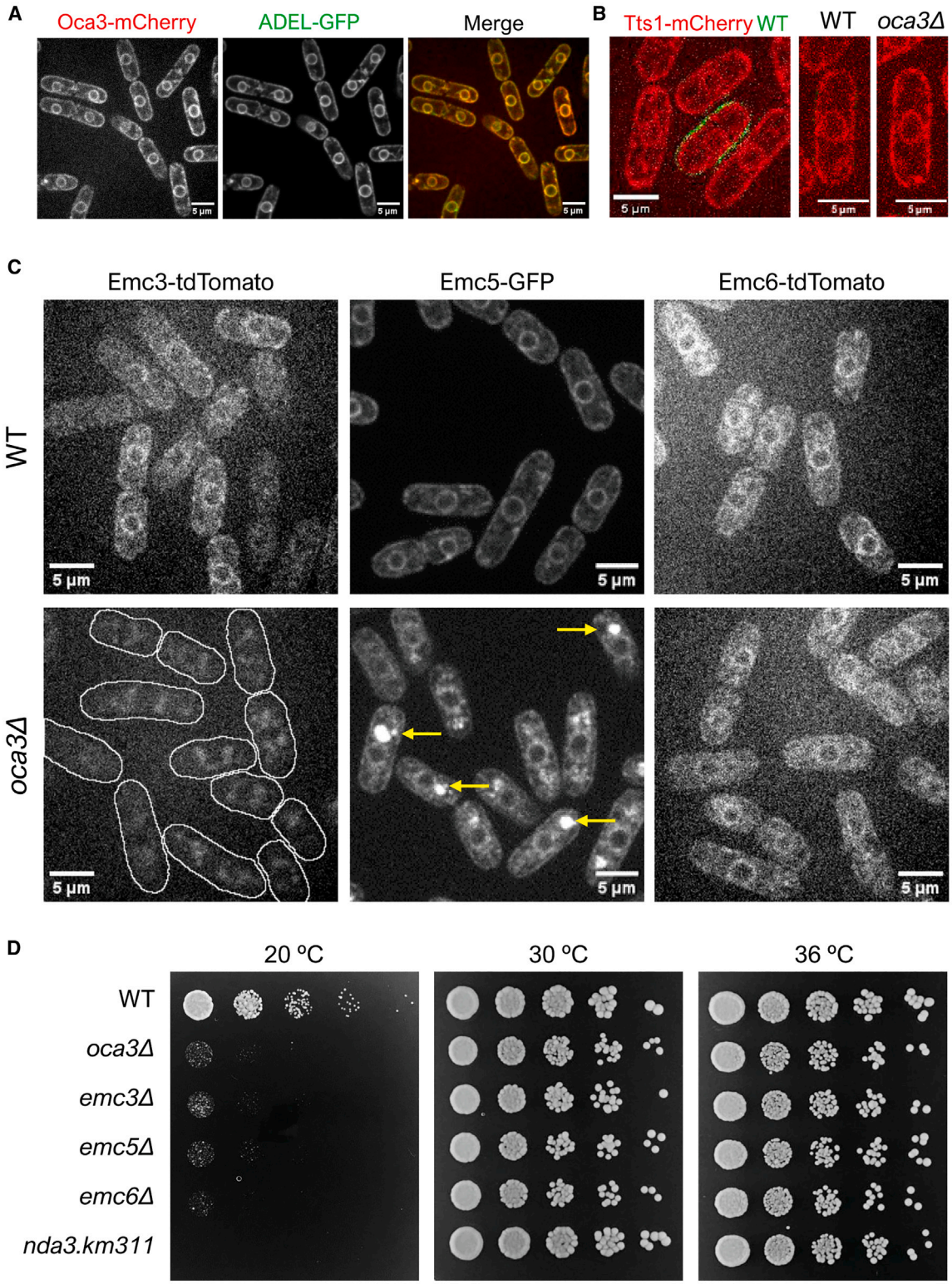

Figure 1. Genetics analysis of EMC complex proteins

(A) Subcellular localization Oca3-mCherry (left panel) and the ER reporter ADEL-GFP (central panel). Merge image is shown (right panel).

(B) Membrane organization of *oca3Δ* mutant cells compared to *wild-type* cells. Fluorescent images of Tts1-mCherry, located in most subcellular membranes (*wild-type* control cells are stained with green lectin).

(legend continued on next page)

the ADEL-GFP fusion, a bona-fide ER marker.[13] As expected for an EMC component, *in vivo* fluorescence microscopy shows that Oca3-mCherry localizes to the ER (Figure 1A), co-localizing with the ER-reporter ADEL-GFP. Localization of the Tts1-mCherry construct, enriched in the tubular structure of the ER[14] indicates that the ER, ER-associated plasma membrane (PM) and nuclear membrane remain unaltered in *oca3*-null cells (the *oca3Δ* deletion strain) (Figure 1B).

In budding yeasts, the eight subunits of the EMC heterooligomer complex show similar genetic interaction patterns.[1] The cytosolic region of EMC is formed by Emc2 and the cytosolic domains of Emc3, Emc4 and Emc5, whereas Emc1 and Emc3–Emc6 are transmembrane proteins.[15] Like Oca3, localization of fluorescently tagged constructs of the putative orthologous *S. pombe* Emc3 (Pombase: ID SPBC1711.03), Emc5 (Pombase: ID SPAP4C9.02) and Emc6 (Pombase: ID SPCC1020.11c) is consistent with the ER structure in all these EMC subunits. As shown in Figure 1C, depletion of Oca3 leads to loss of Emc3, aggregation of Emc5, and normal ER localization, but reduced fluorescence levels of EMC6, revealing the requirement of Oca3 for the assembly of a functional EMC complex.

The *oca3Δ* strain produces compromised cells that can grow at 30°C but fail to grow at lower temperatures (routinely assessed at 20°C) (Figure 1D), a cold-sensitive phenotype that may reflect the loss of membrane lipid homeostasis,[16,17] energy homeostasis,[18,19] or other adaptive mechanisms required for growth at these environmental conditions. Likewise, the deletion of genes encoding the above predicted components of the *S. pombe* EMC (*emc3Δ*, *emc5Δ* and *emc6Δ*) renders a cold-sensitive phenotype too (Figure 1D).

Taken together, we conclude that the *oca3* gene encodes the eukaryotic EMC2 ortholog found in *S. pombe* (Oca3/Emc2), the deletion of this gene driving to EMC-deficient cells.

EMC deficiency leads to mitochondrial dysfunction

Depletion of Oca3/Emc2 leads to severe growth defects at low temperature. To determine possible roles of EMC in *S. pombe* cell growth, we first analyzed nuclear and mitochondrial DNA in DAPI-stained cells under permissive (30°C) and restrictive (20°C) growth conditions. In comparison to the wild-type control, no significant alterations in nuclear staining were observed in *oca3Δ* cells; however, clumps of mitochondrial DNA (mtDNA) were present in the cytoplasm of these mutant cells (Figure 2A). Quantitative PCR analysis of target mtDNA sequences determined a 28% reduction in mtDNA molecules per cell in the mutant strain at 30°C, exacerbated at low temperature (37% reduction at 20°C) (Figure 2B). This result suggests that EMC may be required for the proper organization and/or stability of mtDNA during its replication/segregation cycle.

Depletion of Oca3/Emc2 leads to severe growth defects at low temperature. One potential cause is impaired mitochondrial structure-function, which may include reduced energy production due to disrupted oxidative phosphorylation or compromised mitochondrial beta-oxidation of fatty acids. These processes are essential for maintaining energy homeostasis under stress conditions and are particularly vulnerable at restrictive temperatures.[18,19] To determine whether mtDNA aggregations generated in *oca3Δ* cells are accompanied by alterations in the mitochondrial structure, mtDNA and mitochondrial membranes were stained using Hoechst and MitoTracker, respectively, and cells were analyzed under the microscope. In comparison to *wild-type* cells, Oca3/Emc2 depletion results in a condensed mitochondrial structure that co-localize with abnormal mtDNA aggregations (Figure 2C). *In vivo* visualization of the mitochondrial lumen (the Arg11-mCherry marker) reveals severe morphological alterations of mitochondria (Figures 2D and 2E) in EMC-deficient cells, while this morphology remains unaltered in *wild-type* cells independently of the temperature (see in Figure 2D).

The accumulation of reactive oxygen species (ROS) is associated to mitochondrial dysfunctions.[18] Remarkably, proliferating Oca3-depleted cells (at 30°C) reach ROS levels similar to those found in *wild-type* cells subjected to oxidative stress (H_2O_2 treatment), indicating that EMC-deficient cells suffer mitochondrial stress (Figures S1A and S1B). The addition of N-Acetylcysteine (NAC), a compound known to act as a reducing agent and protect cells from excess ROS,[20] slightly reduces ROS accumulation and partially restores growth of *oca3Δ* cells at 20°C (Figure S1C), suggesting that mitochondrial dysfunction, among other reasons, is likely compromising the survival of these EMC-deficient cells. Overall, we conclude that EMC is required for mtDNA stability and normal mitochondria structure and function.

Oca3/Emc2 depletion impairs the biogenesis of ER-mitochondria tethering factors

ER membranes show normal structure in *oca3Δ* cells (see in Figure 1). Therefore, mitochondrial aggregates observed in these mutant cells suggest that mitochondrial membranes are largely detached from ER membranes. Interestingly, the defective mitochondrial structure observed in *oca3Δ* mutant cells (Figures 2D and 2E) resembles that reported in mutants with reduced ER-mitochondrial tethering,[19] suggesting also a role for EMC in ER-mitochondria tethering in *S. pombe*, as reported in mammals and budding yeasts.[21,22] However, EMC anchoring functions could be exerted indirectly, by assisting the biogenesis of ER-mitochondria docking factors such as ERMES (ER–mitochondria encounter structure)[20,23] or Lam6/Ltc1, a TMD-protein that enables sterol trafficking at ER-PM and ER-vesicles contacts in *S. pombe* cells[17] and the ER-mitochondria and ER–vacuole contact sites in *S. cerevisiae.*[24]

To further study the possibility that tethering complexes could be included in the wide range of putative EMC clients,[25] the ERMES complex subunit Mdm34[26] and Ltc1[17] were tagged with GFP, and their subcellular localization was analyzed by time-lapse microscopy in *wild-type* and *oca3Δ* cells at 30°C

(C) Subcellular localization of Emc3-tdTomato, Emc5-GFP and Emc6-mCherry subunits of the EMC complex in *wild-type* and *oca3Δ* genetic background. In *oca3Δ* cells, Emc3 is missing from the ER (lines are used to shape cells), Emc5 forms aggregates (arrows) and Emc6 decreases fluorescence intensity.
(D) Spot growth test (sequential 5-fold dilutions) of *oca3Δ*, *emc3Δ, emc5Δ,* and *emc6Δ* strains, along with *wild-type* (wt) and *nda3.km311* (cold-sensitive control) at 20°C, 30ºC and 36°. Scale bar 5 μm.

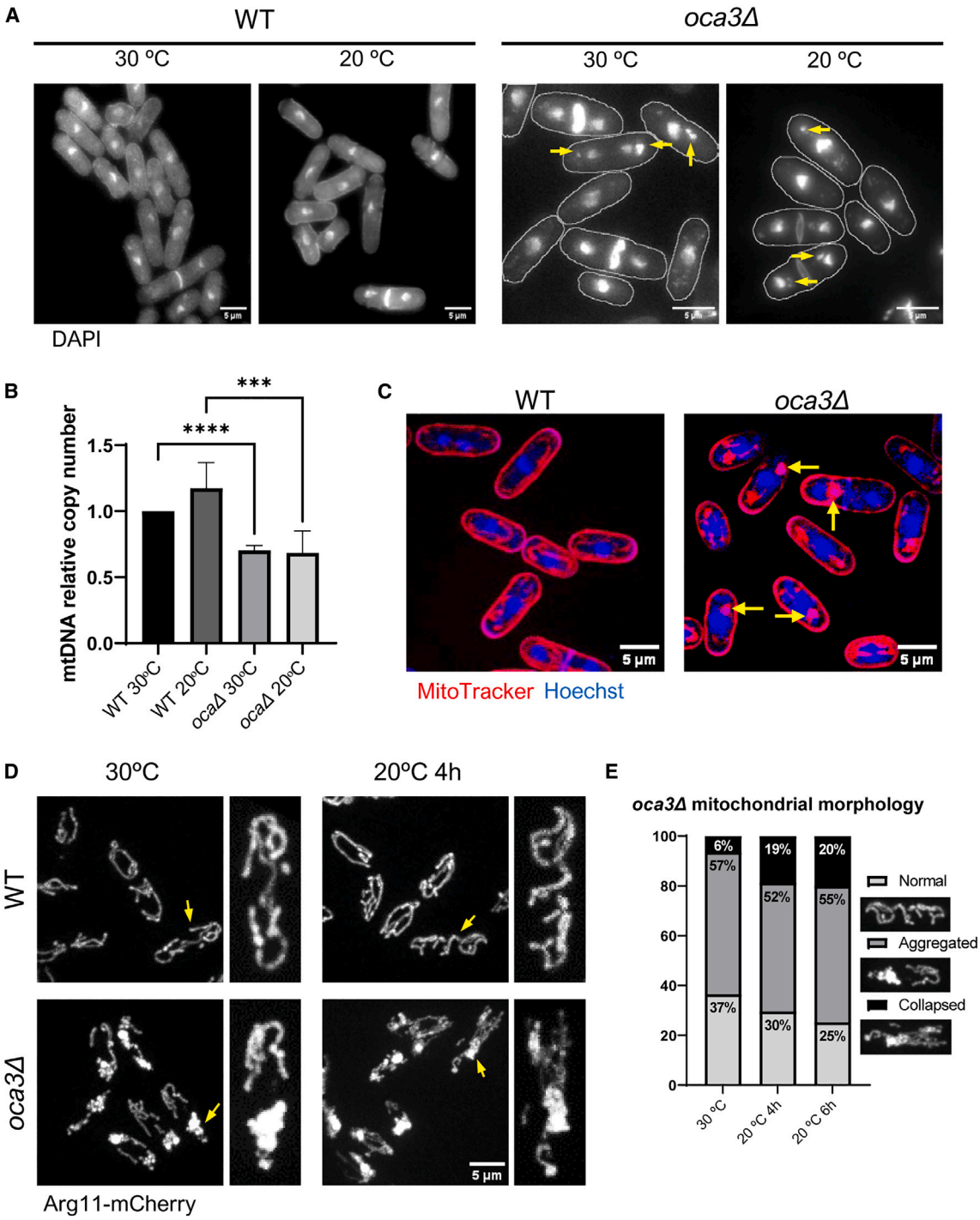

Figure 2. EMC dysfunction alters mitochondrial structure and function

(A) DNA visualization (DAPI staining) at permissive (30°C) and restrictive (20°C after 6h incubation) growth temperatures. Arrows indicate DNA aggregates outside the nucleus. Images are maximal projections of stacks of 0.5 µm layers.

(B) mtDNA copy number/cell quantified by qPCR in *oca3Δ* and *wild-type* (wt) cells at 30°C and 20°C. Statistical significance is indicated (***p value < 0.005, ****p value < 0.001 calculated by the Student's t test). Data are normalized to *wild-type* (wt) and represented as mean; error bars represent the standard deviation (SD) of three independent experiments.

(C) Fluorescence images obtained from DNA (Hoechst) and mitochondria (MitoTracker) staining of *wild-type* (wt) and Oca3-depleted cells at 30°C. Mitochondrial membranes and mtDNA aggregations co-localize (arrows).

(legend continued on next page)

and 20°C. As shown in Figure 3, Mdm34-GFP co-localizes with mitochondrial membrane markers in *wild-type* cells, enriched at the ERMES ER-mitochondrial contact sites.[27] In *oca3Δ* cells, most of the Mdm34-GFP is delocalized into the abnormal mitochondria, indicating that EMC disfunction may interfere the assembly of ERMES components. But eventually, patches of Mdm34-GFP are still observed in the outer membrane in the remaining mitochondrial tubular structures of this mutant (see in Figure 3), suggesting that EMC is not essential for ERMES assembly. Loss of ERMES function is lethal in *S. pombe*,[19] suggesting that the fraction of this complex found at ER-mitochondria contacts is still functional (see Figure 3).

In agreement with its localization in ER-PM and ER-vesicles previously described in fission yeast,[17] Ltc1-GFP localizes to cortical and internal dots in the ER in *wild-type* cells (arrows in Figure 3), but MitoHealth co-localization indicates that this protein is also associated to ER-Mitochondrial contact sites in *S. pombe* cells (Figures 3 and S2), as reported in *S. cerevisiae* cells.[24] In contrast to Mdm34-GFP, Ltc1-GFP lacks its normal ER-PM and ER-mitochondria localization (see Figure 3). This result indicates that Ltc1 localization is fully dependent on EMC activity.

Interestingly, Ltc1-GFP delocalizes from the ER-membrane contact sites to decorate the matrix of the mitochondrial aggregates in *oca3Δ* cells (see in Figure 3). The sequestration of Ltc1-GFP into the mitochondria in these cells can be attributed to the mitochondria-associated proteostatic mechanism for unfolded proteins in the ER (ER-associated mitochondrial sequestration, ERAMS).[28] We therefore conclude that Ltc1 may be a client of EMC, whose proper folding and biogenesis in the ER could be driven by the EMC. Overall, our results suggest that EMC may be involved in ER-mitochondrial tethering by favoring folding and insertion of ERMES and by assisting Ltc1 biogenesis.

EMC regulates ergosterol homeostasis by assisting Ltc1 biogenesis

The EMC complex has emerged as an important eukaryotic complex for homeostasis of sterols.[6,9] Since *S. pombe ltc1Δ* mutant cells lead to the overaccumulation of ergosterol in yeast cell membranes,[17] we wondered whether Ltc1 delocalization (Figure 3) also resulted in overaccumulation of ergosterol in the *oca3Δ* strain.

To determine whether EMC is involved in ergosterol homeostasis in *S. pombe* cells, sterols were extracted from cells incubated at 20°C and 30°C and the amount of ergosterol was quantified by TLC silica gel. As shown in Figure 4A, loss of EMC results in a marked increase in the ergosterol content in the *oca3Δ* mutant strain at both temperatures when compared to levels in *wild-type* cells. Increased levels are also observed by fluorescent quantification of sterol droplets using the D4H probe[17] (Figure 4B).

Physiological assays were also used to confirm these analytical results. Nystatin specifically binds ergosterol in the yeast PM creating pore-forming complexes that result in cell death.[29] Consequently, mutants that reduce ergosterol content are particularly resistant to the effects of nystatin,[30] whereas high ergosterol levels render cells more sensitive to the effects of the drug.[31] On the contrary, cells that accumulate excess ergosterol are highly resistance to ketoconazole, a drug that reduces ergosterol content by inhibiting its biosynthesis.[32] As expected for the observed ergosterol overaccumulation (Figures 4A and 4B), the growth of Oca3/Emc2-depleted cells is sensitive to nystatin and resistant to ketoconazole (Figure 4C). Since Ltc1 requires EMC for its localization and function at ER-Plasma membrane and ER-mitochondria contact sites (Figure 3), we conclude that EMC regulates ergosterol homeostasis through the ER-assisted biogenesis of the sterol transfer protein Ltc1.

Strikingly, ketoconazole rescues the cold-sensitive growth phenotype of Oca3/EMC2-depleted cells (see in Figure 4C), indicating that ergosterol overaccumulation is indeed a major cause of the detrimental growth of these *oca3Δ* cells. Equivalent results were reported in mammals, where the excess cholesterol (the equivalent to ergosterol in mammals) in EMC-depleted mutants leads to cell death.[6]

Membrane fluidization rescues cell functions in EMC-deficient cells

The cold-sensitive growth rescued by ketoconazole indicates that the surplus ergosterol largely accounts for growth defects of Oca2/Emc2-depleted cells at low temperature (20°C) (see Figure 4C). Ergosterol (cholesterol in higher eukaryotes) is a cell membrane-rigidizing molecule,[33,34] its homeostatic regulation being necessary to maintain optimal lipid bilayer fluidity under environmental changes.[16,35–37] Sterol overaccumulation rigidizes cell membranes and interferes with membrane-associated processes, thereby contributing for cold-sensitiveness in yeasts.[16,17] Therefore, we hypothesized that upon ergosterol overaccumulation, membrane fluidity in *oca3Δ* cells is below the survival threshold at 20°C. The increase in fluidity with temperature may counteract this rigidifying effect thereby providing a permissive growth condition for this mutant strain at high temperature (assessed at 30°C and 36°C) (Figures 1D, 2A, and 4C). To further investigate this idea, we analyzed the effects on growth of different membrane-fluidizing agents (detergents and alcohols)[38–40] in *oca3Δ* cells. As shown in Figure 5A, ethanol, a membrane fluidizer at intermediate concentrations[40,41] partially suppresses sensitive growth at 20°C in this strain. Sorbitol shows similar results, but the non-ionic detergent Tween 20 is surprisingly efficient in rescuing cold-sensitive growth of *oca3Δ*

(D) *in vivo* Arg11-mCherry localization (mitochondrial lumen marker) in *oca3Δ* (lower panels) and the *wild-type* control (upper panels) cells at 20°C (right panels) and 30°C (left panels). Deletion of *oca3* condensates the mitochondrial structure resulting in viable mitochondrial aggregation at 30°C. The phonotype is exacerbated after 4h at 20°C where the mitochondrial network collapses (arrows and enlargements).

(E) Quantification of mitochondrial Arg11-mCherry fluorescence (see STAR Methods). Representative cells with either normal, aggregated and or collapsed mitochondria structures are shown. High proportion of collapsed mitochondrial membranes after 4h (19%, n = 176 cells) and 6h (20%, n = 95 cells) incubation at 20°C (restrictive growth temperature), as compared to cells incubated at 30°C (permissive growth temperature) (6%, n = 93 cells), is observed. Only normal mitochondria are found in the analyzed sample of *wild type* cells (100% normal, not represented). Scale bars 5 μm.

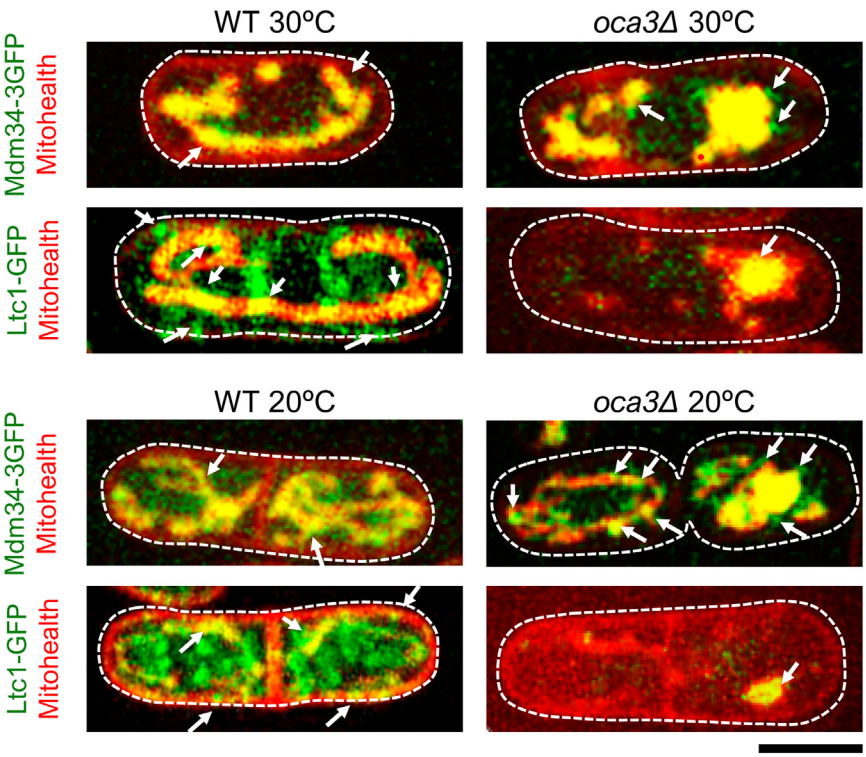

Figure 3. ERMES and Ltc1 subcellular localization

Fluorescence images of the ERMES subunit Mdm34-3GFP and Ltc1-GFP in *wild-type* (wt) and *oca3Δ* representative cells at 30°C (top panels) and 20°C (lower panels). MitoHealth (red) and GFP (green) fluorescence are used in the same cells (merge images) to highlight mitochondrial and PM membrane localization and co-localization (yellow). Scale bar 5 μm.

cells (Figures 5A and 5B). At this temperature (20°), ergosterol content is low in *wild-type* cells, but increases in media with Tween 20 (Figure 5C), as expected for the homeostatic response to counteract the fluidizing effects of this solvent. EMC-deficient cells lack ergosterol homeostasis, and ergosterol levels remain high regardless of Tween 20 addition and growth temperature (20°C and 30°C) (Figure 5C). Therefore, as temperature, Tween 20 likely rescues cold-sensitive growth of EMC-deficient cells through its fluidizing properties, by counteracting membrane rigidizing of surplus ergosterol in these mutant cells, rather than by reducing its membrane content (as ketoconazole).

To estimate *in vivo* fluidizing effects of Tween 20 on ergosterol enriched membranes of Oca3/Emc2-depleted cells, fluorescence recovery after photobleaching (FRAP) assays were carried out to study lateral diffusion of Scs2-GFP (ER/PM protein),[42] and Ish1-GFP (nuclear envelope)[43] in proliferating *S. pombe* cells (30°C). As shown in Figure 5D, the lateral diffusion rate of both markers is reduced in *oca3Δ* cells, but importantly, the diffusion rate is recovered to *wild-type* values by addition of Tween 20 (0.04%) in these mutant cells. Thus, the fluidizing properties of this non-ionic detergent most likely rescue growth defects in Oca3/Emc2-depleted cells by *in vivo* counteracting the rigidizing effects of excess ergosterol.

Under proliferating growth conditions (30°C), Oca3/Emc2-depleted cells aggregate the mitochondria (Figures 2D and 2E) and decrease levels of mtDNA molecules (Figure 2B). In addition to cold-sensitive growth, we show that Tween 20 significantly rescues the defective mitochondrial tubular network (Figure 5E) and mtDNA content (Figure 5F). Overall, our results indicate that non-optimal membrane fluidity is an important biophysical contributor to the pleiotropic defects observed in Oca3/Emc2-depleted cells. Furthermore, this result underlines a major role of the EMC complex in membrane fluidity homeostasis by regulating ergosterol levels in *S. pombe* cells through Ltc1 biogenesis.

Membrane rigidity hinders folding of ER membrane proteins

How fluidization of cell membranes with surplus ergosterol rescues cold-sensitive growth and mitochondrial dysfunctions in EMC-deficient cells is intriguing. EMC is expected to assist folding at the ER of a still incomplete set of ER membrane proteins.[5,9,21,44] To estimate the levels of ER-unfolded proteins in EMC-deficient cells, we monitored fluorescence intensity in proliferating cells (30°C) expressing the ER-reporter mCherry-ADEL under the promoter of the BiP1/GRP78 protein, an abundantly expressed Hsp70 family member specifically induced by the unfolded protein response (UPR).[45–47] As shown in Figure 6A, basal levels of mCherry ADEL expression decorate the ER-membranes of *wild-type* cells. In contrast, BiP1-driven expression of mCherry-ADEL is greatly induced in Oca3/Emc2-depleted cells. The UPR senses the protein folding capacity of the ER,[45] suggesting that EMC dysfunction may provoke the accumulation of ER-unfolded proteins in *S. pombe* cells (ER stressed cells).

Surprisingly, Tween 20 reduces BiP1-driven mCherry-ADEL expression by approximately 20% in these Oca3/Emc2-depleted cells. In mammalian cells, cholesterol can directly activate the UPR,[48] suggesting that surplus ergosterol in this strain may also be directly activating the UPR signal in *S. pombe* cells. Accordingly, the reduction in BiP1 expression is even greater (37% on average) with the addition of ketoconazole (see Figure 6A). However, a significant UPR signal is still observed in ketoconazole treated cells, underlying that in addition to ergosterol, a set of unfolded proteins which requires direct assistance of EMC for proper folding may be activating the unfolded-protein response.

Biogenesis of transmembrane proteins is modulated by membrane lipid composition.[49] We therefore conclude that in the absence of EMC function, ergosterol rigidized membranes impair proper folding of a significant fraction of membrane proteins at the ER, which is permitted (spontaneously or assisted by other chaperones) under optimal membrane fluidity conditions. Furthermore,

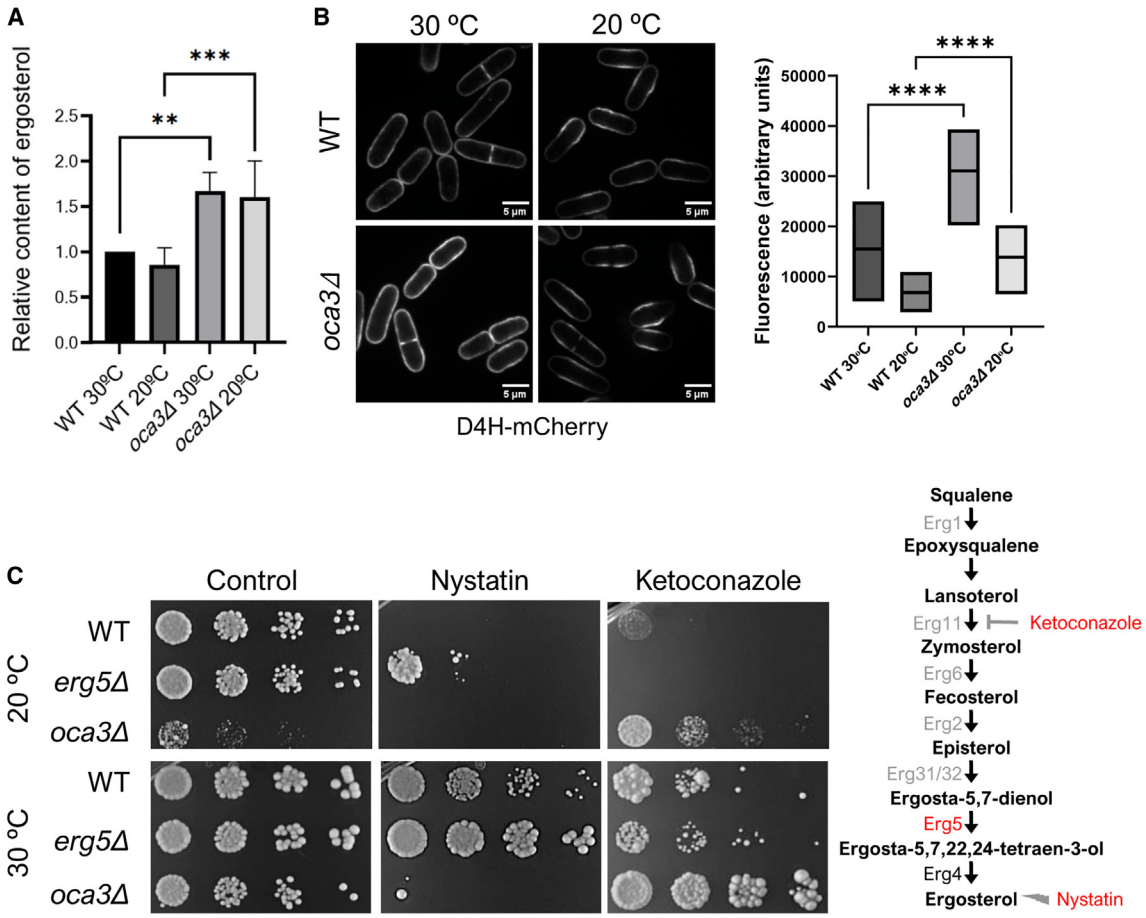

Figure 4. Overaccumulation of ergosterol in the *oca3Δ* mutant strain

(A) Quantification of ergosterol content by TLC analysis in *oca3Δ* and *wild-type* (wt) control cells at 20°C and 30°C. Statistical significance is indicated (**p value < 0.01, ***p value < 0.005 calculated using one-way ANOVA). Data are normalized to *wild-type* (wt) at 30°C and represented as mean; error bars represent the SD of three independent experiments.

(B) Fluorescence images of the D4H-mCherry marker in *wild-type* (wt) at 20°C (n = 64 cells) and 30°C (n = 63 cells) and *oca3Δ* cells at 20°C (n = 76 cells) and 30°C (n = 38 cells). Scale bar 5 μm. Fluorescence quantification of these cells is shown (right panel) (****p value < 0.001 calculated using one-way ANOVA). Data are represented as mean +/− min and max.

(C) Spot growth assay (sequential 5-fold dilutions) of *wild-type* (control) and *oca3Δ* strains at 20°C and 30°C on control plates (EMM2) and plates containing nystatin (5 μg/mL) and ketoconazole (0.2 μM). The *erg5Δ* strain, which disrupts the ergosterol synthesis[30] is used as control. Steps affected by *erg5Δ,* ketoconazole and nystatin are highlighted in the ergosterol biosynthesis pathway.

our results give EMC a key role in membrane fluidity homeostasis to favor membrane protein folding.

In view of this result, we analyzed the localization of Ltc1-GFP and Mdm34-3GFP in *oca3Δ* cells upon addition of Tween 20. As shown above (Figure 5E), this non-ionic detergent significantly rescues defects in the tubular structure of mitochondria, but Ltc1-GFP remains depleted from ER-PM and ER-mitochondrial contact sites (Figures 6B and S3). Accordingly, ergosterol level remains high in Tween 20 treated *oca3Δ* cells (Figure 5C).

Ltc1 overexpression[17] does not recue cold-sensitive growth in *oca3Δ* cells, albeit the combination of both causes a significant synthetic growth defect compared with deletion of *oca3* alone (Figure 6C). Therefore, Ltc1 requires EMC activity independently of the membrane fluidity, and recovery of the mitochondrial structure cannot be directly attributed to a tethering role of Ltc1. To our acknowledgment, the assembly and function of ERMES in ER-mitochondrial contact sites is not dependent on EMC activity. However, Mdm34-3GFP expands as the tubular structure of mitochondria is recovered in the presence of Tween 20 (see in Figures 6B and S3). The same results were obtained by ketoconazole treatment of *oca3Δ* cells (see in Figures 6B and S3). These observations lead us to conclude that EMC assists membrane protein folding and insertion by direct action on client proteins (i.e., Ltc1), but also may facilitate the biogenesis of some other membrane proteins by providing optimal membrane fluidity (i.e., ERMES components). Structure-based functional studies distinguish between two separable EMC activities, as an insertase regulating tail-anchored TMD proteins and a broader role in polytopic membrane protein biogenesis.[50] Perhaps these two activities could be related to the direct and

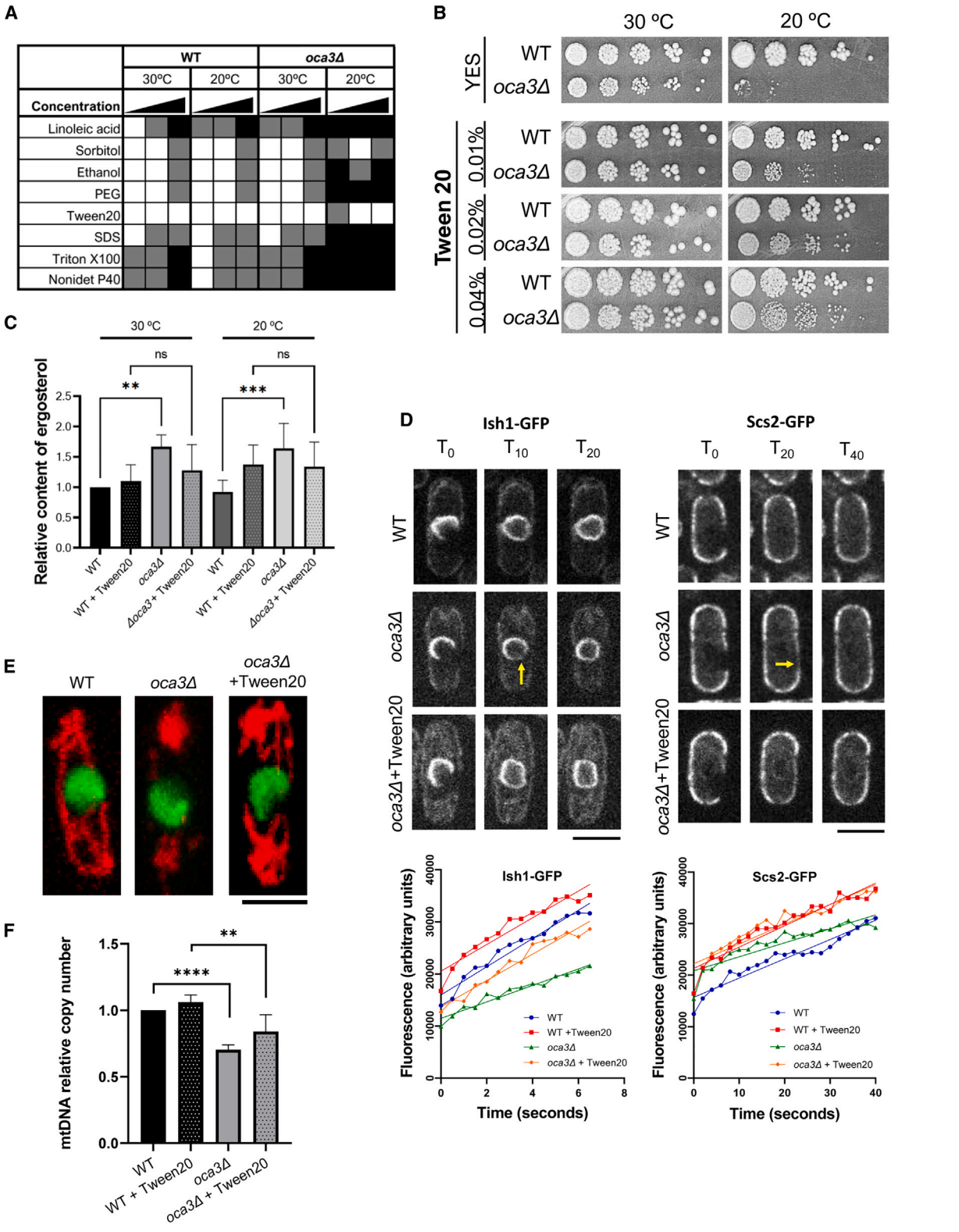

(legend on next page)

assisted biogenesis of distinct client protein classes described above.

DISCUSSION

Pleiotropic outcomes of EMC disruption arise from membrane rigidizing effects of surplus ergosterol

The EMC complex assists the folding and insertion of TMD-containing proteins at the ER with specific topologies so that they carry out their activities.[21] Given the large proportion of genes encoding membrane proteins, a central role for EMC as a TMD chaperone and insertion factor may explain its high abundance, broad conservation, and pleiotropic phenotypes.[9,51] Accordingly, we observed that *S. pombe* cells losing EMC function constitutively overaccumulate ergosterol (Figures 4A and 4B) and show cold-sensitive growth (Figures 1D, 2A, and 4C) and severe mitochondrial dysfunctions (Figures 2D, 2E, and 3).

Interestingly, in the routinary ketoconazole resistance assay to confirm the excess of ergosterol,[32] we observed that this drug recues both cold-sensitivity of growth (Figure 4C) and mitochondrial dysfunctions in EMC-deficient cells (see in Figures 5E and 6B). To our surprise, the non-ionic detergent Tween 20 equally rescues cold-sensitive growth and mitochondrial dysfunctions, as well as ER stress, in these mutant cells (Figures 6A, 6B, and S3). In all eukaryotes, cholesterol/ergosterol homeostasis is part of the adaptive mechanisms that maintain optimal cell membrane fluidity under changing environments.[33,34] Decreased levels of EMC clients may impact in their functions in EMC-deficient cells.[9] Nonetheless, in *S. pombe* EMC-deficient cells, we demonstrate that the pleiotropic phenotypic defects observed in EMC-deficient cells mainly arise from non-optimal membrane fluidity caused by the excess of ergosterol.

EMC drains membrane ergosterol via the sterol transfer protein Ltc1

Sterols serve for membrane integrity and proper activity of multiple membrane proteins,[52] but importantly, sterol homeostasis is essential to attain optimal fluidity of cell membranes.[53,54] In mammals, a key step in this system involves the transport of sterols from the PM to the ER and from the ER to the mitochondria, where it is metabolized to 27-hydroxycholesterol that rapidly exits the cell.[34,55–57] Disruption of this flow pathway drives to the overaccumulation of this sterol upstream of the ER-mitochondrial transit step.[58]

In *S. pombe*, the sterol transfer Ltc1 plays a major role in the ergosterol flux across ER-PM contact sites, where it resides[17] (Figures 3 and 6B). Here, we show that Ltc1 also localizes to ER-mitochondrial membrane contacts (Figures 3 and 6B). Thus, as previously reported in *S. cerevisiae* cells,[24] this protein may also facilitate ergosterol transfer from the ER to the mitochondria. Since Ltc1 depletion leads to ergosterol overaccumulation in *S. pombe* cells,[17] it is likely that sterol transport from the PM to the ER and from the ER to the mitochondria by this protein is required to drain ergosterol excess in these cells.

Ltc1 contains a C-terminal TMD required to localize at sites of sterol transport,[24] a domain that fits requirements for EMC-clients.[50] It is noteworthy that the localization of Ltc1 in contact sites between the ER and the PM and between the ER and the mitochondria depends on the activity of the EMC (see in Figures 3 and 6B). The EMC complex promotes biogenesis of sterol-related enzymes maintaining sterol homeostasis in mammalian cells.[6] We show here that in *S. pombe* cells, proper folding and insertion of Ltc1 by this complex also plays a key role in sterol homeostasis, and in turn in membrane fluidity, perhaps draining sterol by a pathway similar to that found in mammal cells.[34,55–57] The recent finding of a tripartite membrane contact site between the PM, ER, and mitochondria[59] may facilitate the flow of sterols from the PM to the ER and then from the ER to mitochondria.

Unfolded Ltc1 delivery into the mitochondria

During the biogenesis of TMD-membrane proteins, unfolded protein species eventually arise during EMC-mediated maturation that require clearance from the ER membrane.[9,59] EMC components show close interaction with the ERAD machinery.[8,60] Accordingly, quantitative proteomic methodologies identified putative EMC clients, including some of its own subunits, by significant depletion in EMC-deficient cells (i.e., EMC3 in Figure 1C).[5,44] However, other membrane proteins in these cells are not correctly folded but not degraded.[51] This set of non-degraded EMC clients likely uses ERAMS (ER-associated mitochondrial sequestration) rather than ERAD to clear unfolded proteins.[28] As described here, the sterol transfer

Figure 5. Chemical suppression of oca3Δ defects by membrane fluidifying compounds

(A) Effects on growth of *oca3Δ* cells by the indicated chemicals at increasing concentrations. White indicates viability while black represents lethality.

(B) Spot growth assay of *wild-type* (wt) and *oca3Δ* cells at the indicated Tween 20 concentration (%v/v) and temperature (20°C and 30°C) (control media YES is used). Tween 20 (0,02–0.04% v/v) efficiently restores viability of *oca3Δ* cells at 20°C.

(C) Quantification of ergosterol content by TLC analysis in *wild-type* and *oca3Δ* cells in the presence of Tween 20 (0.04%) at 20°C and 30°C (squared graph). Data from control experiments without this solvent are included (previously shown in Figure 4A) (**p value < 0.01, ***p value < 0.005, ns: not significant, calculated using one-way ANOVA). Data normalized to *wild-type* (wt) at 30°C and represented as mean; error bars represent the SD of three independent experiments.

(D) Fluorescence recovery by lateral diffusion of the nuclear envelop inserted Ish-GFP after Photobleaching (left) and the plasma membrane/ER inserted Scs2-GFP protein (right) in *wild-type* and *oca3Δ* cells with and without Tween 20 as indicated. Scale bars 5 μm. Their fluorescent recovery dynamics (graphs) are shown. The slopes in fluorescence recovery dynamics are significantly different between *wild-type* and *oca3Δ* cells in both Ish1-GFP (p value < 0.001) and Scs2-GFP (p value < 0.01), while no significant differences are observed between *wild-type* and *oca3Δ* cells with Tween 20 in either Ish1-GFP (p value = 0.65) or Scs2-GFP (p value = 0.6) according to the Student's t test. N = 9 for each condition, data are represented as a regression fit of the mean.

(E) Representative image of nuclear DNA (green) and the membrane mitochondrial network (red) of *wild-type*, *oca3Δ* cells and *oca3Δ* cells with Tween 20 (0.04% v/v) at 20°C and 30°C. Reduced aggregations and the recovery of tubular membranes in the mitochondrial network of *oca3Δ* cells with Tween 20 indicates a partial recovery of *wild-type* structures by this non-ionic detergent (arrows). Scale bars 5 μm.

(F) mtDNA copy number/cell quantified by qPCR in cells of *the* indicated strains at 30°C in the presence of Tween 20 (0.04%) or without this detergent. Statistical significance is indicated (**p value < 0.01, ****p value < 0.001 calculated by the Student's t test). Data are normalized to *wild-type* (wt) and represented as mean; error bars represent the SD of three independent experiments.

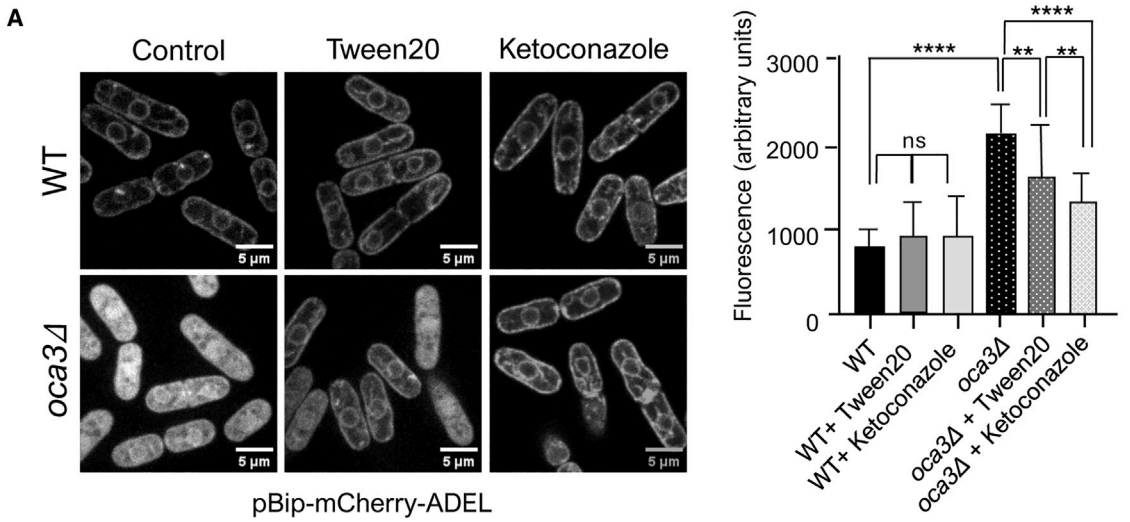

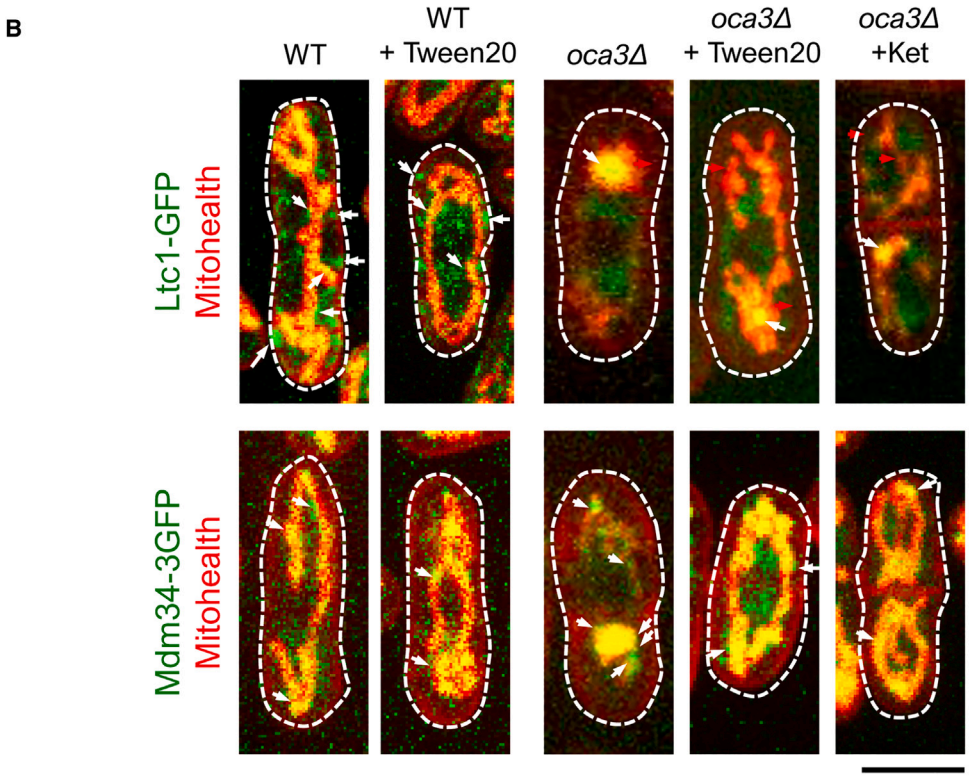

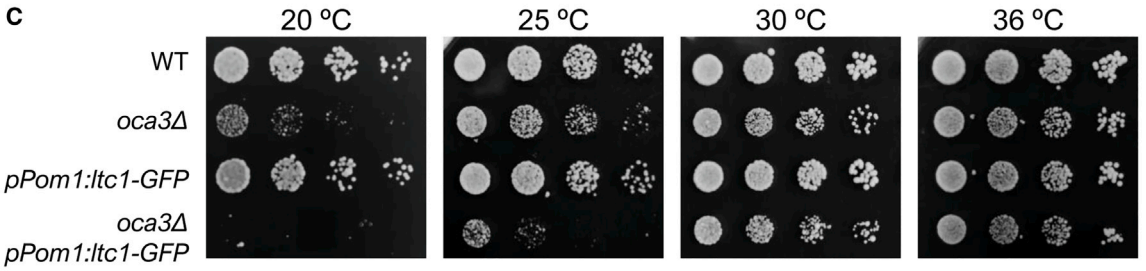

(legend on next page)

protein Lam6/Ltc1 belongs to this set of proteins that, in the absence of EMC, is delivered to the mitochondrial matrix for the sequestration of unfolded proteins. Unfolded proteins may also come from membrane-associated proteins that requires optimal membrane fluidity for proper folding (i.e., Mdm34) (Figures 3 and 6B). In agreement with the high UPR signal in EMC-deficient cells (ER stress) (Figure 6A), we propose that accumulation of these unfolded proteins provoke mitochondria stress and swollen it to the point that ruptures seams at ER-mitochondrial junctions (Figures 2D, 3, and 6B). Membrane fluidization by Tween 20 in these cells facilitates folding and relieves mitochondrial stress to support the recovery of tubular structure and ER-mitochondrial binding factors (mainly ERMES). ER-mitochondria contacts couple mtDNA synthesis with mitochondrial division in human cells.[61] The loss of mtDNA in EMC-deficient cells and its partial recovery with Tween 20 may also respond to loss and recovery of ER-mitochondrial contact sites in *S. pombe* cells (Figures 2B and 5F respectively).

Whether the loss of the tubular mitochondrial network in EMC-deficient cells is due to the role of EMC on the tethering functions of Ltc1 and/or ERMES, or the consequence of the tension between the ER and the mitochondrial provoked by the accumulation of unfolded proteins at the mitochondrial matrix (or both) remains an open question. But importantly, membrane fluidification significantly recovers both proteostasis and ER-mitochondria tethering in EMC-defective cells (Figure 6), cellular dysfunctions often associated to aging and neurodegeneration.[62–65]

Membrane fluidization with Tween 20 reduces the UPR signal due to EMC inactivation by approximately 20% (Figure 6). Multiple genetic studies in patients with congenital malformations have now suggested that variants in EMC subunits may be at the root of various congenital malformations.[3] Changes in membrane fluidity in these variants with concomitant effects on membrane protein activities often accompany the transition from a healthy to a pathological state.[66] Although deliberate modulation of membrane fluidity with drugs has not been exploited to date, our data suggest that the fluidizing effect of Tween 20 (food additive E432), which counteract sterol rigidity in EMC-deficient cells, challenges conventional approaches to overcome proteostasis-related human defects and may open new insight into potential treatments related to neurodegenerative and EMC-associated diseases.

Limitations of the study

Here, we show that Ltc1 biogenesis in ER membranes is directly dependent on EMC activity. Ergosterol overaccumulation due to Ltc1 dysfunction is at the root of the phenotypic defects observed in EMC-deficient cells. However, the construction and expression of an EMC-independent form of Ltc1 may help to estimate the extent of mitochondrial and growth defects directly attributed to Ltc1 biogenesis by EMC from those caused by other EMC clients.

RESOURCE AVAILABILITY

Lead contact

Further information and requests for resources, strains and reagents should be directed to and will be fulfilled by the lead contact, Juan Jimenez (jimmar@upo.es).

Materials availability

Plasmids and strains generated are available upon request to the lead contact.

Data and code availability

- All data reported in this paper will be shared by the lead contact upon request.
- This paper does not report original code.
- Any additional information required to reanalyze the data reported in this work paper is available from the lead contact upon request.

ACKNOWLEDGMENTS

We thank Dr. Martin for providing D4H probe plasmid and *ltc1*-GFP-tagged strains and Dr. Daga for providing fluorescent tagged strains. This work was supported by the Spanish Ministerio de Ciencia e Innovación (grant number PID2019-111124GB-I00 to J.J.). We thank Katherina García for her assistance in the advanced microscopy facility, Victor Carranco for excellent technical assistance, and all members of the yeast genetics group at the CABD for valuable comments and discussions.

AUTHOR CONTRIBUTIONS

M.B., V.A.T. and J.J. designed the experiments. M.B. performed the experiments and analyzed the data. V.A.T. analyzed the data and supervised experimental protocols. J.J. analyzed the data, acquired funding, and wrote the paper with input from M.B. and V.A.T.

DECLARATION OF INTERESTS

The authors declare no competing interests.

STAR★METHODS

Detailed methods are provided in the online version of this paper and include the following:

- KEY RESOURCES TABLE
- EXPERIMENTAL MODEL AND STUDY PARTICIPANT DETAILS
  - *S. pombe* strains and culture

Figure 6. Tween 20 and ketoconazole decrease the UPR and rescue the mitochondrial accumulation of Ltc1 and Mdm34 in EMC-deficient cells

(A) mCherry-ADEL expressed under the Bip1 promoter in *wild-type* (wt, $n = 44$ cells) and *oca3Δ* ($n = 53$ cells) cells at 30°C (microphotographs) with or without Tween 20 or ketoconazole as indicated. Scale bars 5 μm. Fluorescence quantification of mCherry-ADEL was used to estimate UPR levels (right panel) (**p value < 0.01, ****p value < 0.001, calculated using one-way ANOVA). Data represented as mean; error bars represent the SD.

(B) Representative proliferating cells (30°C) showing fluorescence images of Ltc1-GFP (upper panels) and Mdm34-3GFP (lower panels) in *wild-type* (wt) and *oca3Δ* cells in the presence and absence of Tween 20 or ketoconazole as indicated. MitoHealth fluorescence (red) is used in these cells expressing GFP-tagged proteins to highlight mitochondrial and/or PM membrane co-localization (yellow in merge images). Scale bar 5 μm.

(C) Spot growth assay (sequential 5-fold dilutions) of *wild-type* (control), *oca3Δ*, and strains *pPom1:ltc1-GFP* (moderately overexpressing *ltc1*)[17] and *oca3Δ pPom1:ltc1-GFP* at 20°C, 25°C, 30°C and 36°C as indicated.

SUPPLEMENTAL INFORMATION

Supplemental information can be found online at https://doi.org/10.1016/j.isci.2025.112096.

Received: October 9, 2024
Revised: January 9, 2025
Accepted: February 20, 2025
Published: February 24, 2025

REFERENCES

1. Jonikas, M.C., Collins, S.R., Denic, V., Oh, E., Quan, E.M., Schmid, V., Weibezahn, J., Schwappach, B., Walter, P., Weissman, J.S., and Schuldiner, M. (2009). Comprehensive characterization of genes required for protein folding in the endoplasmic reticulum. Science *323*, 1693–1697. https://doi.org/10.1126/science.1167983.
2. Wiseman, R.L., Mesgarzadeh, J.S., and Hendershot, L.M. (2022). Reshaping endoplasmic reticulum quality control through the unfolded protein response. Mol. Cell *82*, 1477–1491. https://doi.org/10.1016/j.molcel.2022.03.025.
3. Zhu, Q., Zhu, X., and Zhang, L. (2024). ER membrane complex (EMC): Structure, functions, and roles in diseases. FASEB J. *38*, e23539. https://doi.org/10.1096/fj.202302266R.
4. Guna, A., Volkmar, N., Christianson, J.C., and Hegde, R.S. (2018). The ER membrane protein complex is a transmembrane domain insertase. Science *359*, 470–473. https://doi.org/10.1126/science.aao3099.
5. Shurtleff, M.J., Itzhak, D.N., Hussmann, J.A., Schirle Oakdale, N.T., Costa, E.A., Jonikas, M., Weibezahn, J., Popova, K.D., Jan, C.H., Sinitcyn, P., et al. (2018). The ER membrane protein complex interacts cotranslationally to enable biogenesis of multipass membrane proteins. Elife *7*, e37018. https://doi.org/10.7554/eLife.37018.
6. Volkmar, N., Thezenas, M.L., Louie, S.M., Juszkiewicz, S., Nomura, D.K., Hegde, R.S., Kessler, B.M., and Christianson, J.C. (2019). The ER membrane protein complex promotes biogenesis of sterol-related enzymes maintaining cholesterol homeostasis. J. Cell Sci. *132*, jcs223453. https://doi.org/10.1242/jcs.223453.
7. Wideman, J.G. (2015). The ubiquitous and ancient ER membrane protein complex (EMC): tether or not? F1000Res. *4*, 624. https://doi.org/10.12688/f1000research.6944.2.
8. Christianson, J.C., Olzmann, J.A., Shaler, T.A., Sowa, M.E., Bennett, E.J., Richter, C.M., Tyler, R.E., Greenblatt, E.J., Harper, J.W., and Kopito, R.R. (2011). Defining human ERAD networks through an integrative mapping strategy. Nat. Cell Biol. *14*, 93–105. https://doi.org/10.1038/ncb2383.
9. Volkmar, N., and Christianson, J.C. (2020). Squaring the EMC - how promoting membrane protein biogenesis impacts cellular functions and organismal homeostasis. J. Cell Sci. *133*, jcs243519. https://doi.org/10.1242/jcs.243519.
10. Tallada, V.A., Daga, R.R., Palomeque, C., Garzón, A., and Jimenez, J. (2002). Genome-wide search of Schizosaccharomyces pombe genes causing overexpression-mediated cell cycle defects. Yeast *19*, 1139–1151. https://doi.org/10.1002/yea.902.
11. Rutherford, K.M., Lera-Ramirez, M., and Wood, V. (2024). PomBase: a Global Core Biodata Resource-growth, collaboration, and sustainability. Genetics *227*, iyae007. https://doi.org/10.1093/genetics/iyae007.
12. Gaudet, P., Livstone, M.S., Lewis, S.E., and Thomas, P.D. (2011). Phylogenetic-based propagation of functional annotations within the Gene Ontology consortium. Briefings Bioinf. *12*, 449–462. https://doi.org/10.1093/bib/bbr042.
13. Pidoux, A.L., and Armstrong, J. (1992). Analysis of the BiP gene and identification of an ER retention signal in Schizosaccharomyces pombe. EMBO J. *11*, 1583–1591. https://doi.org/10.1002/j.1460-2075.1992.tb05203.x.
14. Zhang, D., and Oliferenko, S. (2014). Tts1, the fission yeast homologue of the TMEM33 family, functions in NE remodeling during mitosis. Mol. Biol. Cell *25*, 2970–2983. https://doi.org/10.1091/mbc.E13-12-0729.
15. Bai, L., You, Q., Feng, X., Kovach, A., and Li, H. (2020). Structure of the ER membrane complex, a transmembrane-domain insertase. Nature *584*, 475–478. https://doi.org/10.1038/s41586-020-2389-3.
16. Abe, F., and Hiraki, T. (2009). Mechanistic role of ergosterol in membrane rigidity and cycloheximide resistance in Saccharomyces cerevisiae. Biochim. Biophys. Acta *1788*, 743–752. https://doi.org/10.1016/j.bbamem.2008.12.002.
17. Marek, M., Vincenzetti, V., and Martin, S.G. (2020). Sterol biosensor reveals LAM-family Ltc1-dependent sterol flow to endosomes upon Arp2/3 inhibition. J. Cell Biol. *219*, e202001147. https://doi.org/10.1083/jcb.202001147.
18. Zorov, D.B., Juhaszova, M., and Sollott, S.J. (2014). Mitochondrial reactive oxygen species (ROS) and ROS-induced ROS release. Physiol. Rev. *94*, 909–950. https://doi.org/10.1152/physrev.00026.2013.
19. Rasul, F., Zheng, F., Dong, F., He, J., Liu, L., Liu, W., Cheema, J.Y., Wei, W., and Fu, C. (2021). Emr1 regulates the number of foci of the endoplasmic reticulum-mitochondria encounter structure complex. Nat. Commun. *12*, 521. https://doi.org/10.1038/s41467-020-20866-x.
20. Chapela, S.P., Burgos, H.I., and Stella, C.A. (2022). N-Acetyl cysteine improves cellular growth in respiratory-deficient yeast. Braz. J. Microbiol. *53*, 791–794. https://doi.org/10.1007/s42770-022-00705-5.
21. Lahiri, S., Chao, J.T., Tavassoli, S., Wong, A.K.O., Choudhary, V., Young, B.P., Loewen, C.J.R., and Prinz, W.A. (2014). A conserved endoplasmic reticulum membrane protein complex (EMC) facilitates phospholipid transfer from the ER to mitochondria. PLoS Biol. *12*, e1001969. https://doi.org/10.1371/journal.pbio.1001969.
22. Kornmann, B., Currie, E., Collins, S.R., Schuldiner, M., Nunnari, J., Weissman, J.S., and Walter, P. (2009). An ER-mitochondria tethering complex revealed by a synthetic biology screen. Science *325*, 477–481. https://doi.org/10.1126/science.1175088.
23. Kawano, S., Tamura, Y., Kojima, R., Bala, S., Asai, E., Michel, A.H., Kornmann, B., Riezman, I., Riezman, H., Sakae, Y., et al. (2018). Structure-function insights into direct lipid transfer between membranes by Mmm1-Mdm12 of ERMES. J. Cell Biol. *217*, 959–974. https://doi.org/10.1083/jcb.201704119.
24. Murley, A., Sarsam, R.D., Toulmay, A., Yamada, J., Prinz, W.A., and Nunnari, J. (2015). Ltc1 is an ER-localized sterol transporter and a component of ER-mitochondria and ER-vacuole contacts. J. Cell Biol. *209*, 539–548. https://doi.org/10.1083/jcb.201502033.
25. Wu, H., Smalinskaitė, L., and Hegde, R.S. (2024). EMC rectifies the topology of multipass membrane proteins. Nat. Struct. Mol. Biol. *31*, 32–41. https://doi.org/10.1038/s41594-023-01120-6.
26. AhYoung, A.P., Jiang, J., Zhang, J., Khoi Dang, X., Loo, J.A., Zhou, Z.H., and Egea, P.F. (2015). Conserved SMP domains of the ERMES complex bind phospholipids and mediate tether assembly. Proc. Natl. Acad. Sci. USA *112*, E3179–E3188. https://doi.org/10.1073/pnas.1422363112.
27. Lang, A., John Peter, A.T., and Kornmann, B. (2015). ER-mitochondria contact sites in yeast: beyond the myths of ERMES. Curr. Opin. Cell Biol. *35*, 7–12. https://doi.org/10.1016/j.ceb.2015.03.002.
28. Cortes Sanchon, A., Santhosh Kumar, H., Mantovani, M., Osinnii, I., Mateos, J.M., Kaech, A., Shcherbakov, D., Akbergenov, R., and Bottger, E.C. (2021). ER-misfolded proteins become sequestered with

mitochondria and impair mitochondrial function. Commun. Biol. *4*, 1350. https://doi.org/10.1038/s42003-021-02873-w.

29. Szomek, M., Reinholdt, P., Petersen, D., Caci, A., Kongsted, J., and Wüstner, D. (2021). Direct observation of nystatin binding to the plasma membrane of living cells. Biochim. Biophys. Acta Biomembr. *1863*, 183528. https://doi.org/10.1016/j.bbamem.2020.183528.
30. Skaggs, B.A., Alexander, J.F., Pierson, C.A., Schweitzer, K.S., Chun, K.T., Koegel, C., Barbuch, R., and Bard, M. (1996). Cloning and characterization of the Saccharomyces cerevisiae C-22 sterol desaturase gene, encoding a second cytochrome P-450 involved in ergosterol biosynthesis. Gene *169*, 105–109. https://doi.org/10.1016/0378-1119(95)00770-9.
31. Richman-Boytas, C.M., and Parks, L.W. (1989). Effects of sterol alterations on nystatin sensitivity in Saccharomyces cerevisiae. Microbios *59*, 101–111.
32. Cirigliano, A., Macone, A., Bianchi, M.M., Oliaro-Bosso, S., Balliano, G., Negri, R., and Rinaldi, T. (2019). Ergosterol reduction impairs mitochondrial DNA maintenance in S. cerevisiae. Biochim. Biophys. Acta Mol. Cell Biol. Lipids *1864*, 290–303. https://doi.org/10.1016/j.bbalip.2018.12.002.
33. Venables, P., and Russell, A.D. (1975). Nystatin-induced changes in Saccharomyces cerevisiae. Antimicrob. Agents Chemother. *7*, 121–127. https://doi.org/10.1128/AAC.7.2.121.
34. Elustondo, P., Martin, L.A., and Karten, B. (2017). Mitochondrial cholesterol import. Biochim. Biophys. Acta Mol. Cell Biol. Lipids *1862*, 90–101. https://doi.org/10.1016/j.bbalip.2016.08.012.
35. Subczynski, W.K., Pasenkiewicz-Gierula, M., Widomska, J., Mainali, L., and Raguz, M. (2017). High Cholesterol/Low Cholesterol: Effects in Biological Membranes: A Review. Cell Biochem. Biophys. *75*, 369–385. https://doi.org/10.1007/s12013-017-0792-7.
36. Hryniewicz-Jankowska, A., Augoff, K., and Sikorski, A.F. (2019). The role of cholesterol and cholesterol-driven membrane raft domains in prostate cancer. Exp. Biol. Med. *244*, 1053–1061. https://doi.org/10.1177/1535370219870771.
37. Jorda, T., and Puig, S. (2020). Regulation of Ergosterol Biosynthesis in Saccharomyces cerevisiae. Genes *11*, 795. https://doi.org/10.3390/genes11070795.
38. Juliano, R.L., and Gagalang, E. (1979). The effect of membrane-fluidizing agents on the adhesion of CHO cells. J. Cell. Physiol. *98*, 483–489. https://doi.org/10.1002/jcp.1040980307.
39. Jones, R.P., and Greenfield, P.F. (1987). Ethanol and the fluidity of the yeast plasma membrane. Yeast *3*, 223–232. https://doi.org/10.1002/yea.320030403.
40. Goldstein, D.B. (1986). Effect of alcohol on cellular membranes. Ann. Emerg. Med. *15*, 1013–1018. https://doi.org/10.1016/s0196-0644(86)80120-2.
41. Sergent, O., Pereira, M., Belhomme, C., Chevanne, M., Huc, L., and Lagadic-Gossmann, D. (2005). Role for membrane fluidity in ethanol-induced oxidative stress of primary rat hepatocytes. J. Pharmacol. Exp. Therapeut. *313*, 104–111. https://doi.org/10.1124/jpet.104.078634.
42. Ng, A.Q.E., Ng, A.Y.E., and Zhang, D. (2020). Plasma Membrane Furrows Control Plasticity of ER-PM Contacts. Cell Rep. *30*, 1434–1446. https://doi.org/10.1016/j.celrep.2019.12.098.
43. Asakawa, H., Hirano, Y., Shindo, T., Haraguchi, T., and Hiraoka, Y. (2022). Fission yeast Ish1 and Les1 interact with each other in the lumen of the nuclear envelope. Genes Cells *27*, 643–656. https://doi.org/10.1111/gtc.12981.
44. Tian, S., Wu, Q., Zhou, B., Choi, M.Y., Ding, B., Yang, W., and Dong, M. (2019). Proteomic Analysis Identifies Membrane Proteins Dependent on the ER Membrane Protein Complex. Cell Rep. *28*, 2517–2526. https://doi.org/10.1016/j.celrep.2019.08.006.
45. Kimmig, P., Diaz, M., Zheng, J., Williams, C.C., Lang, A., Aragón, T., Li, H., and Walter, P. (2012). The unfolded protein response in fission yeast modulates stability of select mRNAs to maintain protein homeostasis. Elife *1*, e00048. https://doi.org/10.7554/eLife.00048.
46. Ibrahim, I.M., Abdelmalek, D.H., and Elfiky, A.A. (2019). GRP78: A cell's response to stress. Life Sci. *226*, 156–163. https://doi.org/10.1016/j.lfs.2019.04.022.
47. Vitale, M., Bakunts, A., Orsi, A., Lari, F., Tadè, L., Danieli, A., Rato, C., Valetti, C., Sitia, R., Raimondi, A., et al. (2019). Inadequate BiP availability defines endoplasmic reticulum stress. Elife *8*, e41168. https://doi.org/10.7554/eLife.41168.
48. Feng, B., Yao, P.M., Li, Y., Devlin, C.M., Zhang, D., Harding, H.P., Sweeney, M., Rong, J.X., Kuriakose, G., Fisher, E.A., et al. (2003). The endoplasmic reticulum is the site of cholesterol-induced cytotoxicity in macrophages. Nat. Cell Biol. *5*, 781–792. https://doi.org/10.1038/ncb1035.
49. Brambillasca, S., Yabal, M., Soffientini, P., Stefanovic, S., Makarow, M., Hegde, R.S., and Borgese, N. (2005). Transmembrane topogenesis of a tail-anchored protein is modulated by membrane lipid composition. EMBO J. *24*, 2533–2542. https://doi.org/10.1038/sj.emboj.7600730.
50. Miller-Vedam, L.E., Bräuning, B., Popova, K.D., Schirle Oakdale, N.T., Bonnar, J.L., Prabu, J.R., Boydston, E.A., Sevillano, N., Shurtleff, M.J., Stroud, R.M., et al. (2020). Structural and mechanistic basis of the EMC-dependent biogenesis of distinct transmembrane clients. Elife *9*, e62611. https://doi.org/10.7554/eLife.62611.
51. Chitwood, P.J., and Hegde, R.S. (2019). The Role of EMC during Membrane Protein Biogenesis. Trends Cell Biol. *29*, 371–384. https://doi.org/10.1016/j.tcb.2019.01.007.
52. Saheki, Y. (2017). Endoplasmic Reticulum - Plasma Membrane Crosstalk Mediated by the Extended Synaptotagmins. Adv. Exp. Med. Biol. *997*, 83–93. https://doi.org/10.1007/978-981-10-4567-7_6.
53. Howe, V., Sharpe, L.J., Alexopoulos, S.J., Kunze, S.V., Chua, N.K., Li, D., and Brown, A.J. (2016). Cholesterol homeostasis: How do cells sense sterol excess? Chem. Phys. Lipids *199*, 170–178. https://doi.org/10.1016/j.chemphyslip.2016.02.011.
54. Dawaliby, R., Trubbia, C., Delporte, C., Noyon, C., Ruysschaert, J.M., Van Antwerpen, P., and Govaerts, C. (2016). Phosphatidylethanolamine Is a Key Regulator of Membrane Fluidity in Eukaryotic Cells. J. Biol. Chem. *291*, 3658–3667. https://doi.org/10.1074/jbc.M115.706523.
55. Meaney, S., Bodin, K., Diczfalusy, U., and Björkhem, I. (2002). On the rate of translocation in vitro and kinetics in vivo of the major oxysterols in human circulation: critical importance of the position of the oxygen function. J. Lipid Res. *43*, 2130–2135. https://doi.org/10.1194/jlr.m200293-jlr200.
56. Lange, Y., and Steck, T.L. (2020). Active cholesterol 20 years on. Traffic *21*, 662–674. https://doi.org/10.1111/tra.12762.
57. Steck, T.L., Tabei, S.M.A., and Lange, Y. (2021). A basic model for cell cholesterol homeostasis. Traffic *22*, 471–481. https://doi.org/10.1111/tra.12816.
58. Tian, S., Ohta, A., Horiuchi, H., and Fukuda, R. (2018). Oxysterol-binding protein homologs mediate sterol transport from the endoplasmic reticulum to mitochondria in yeast. J. Biol. Chem. *293*, 5636–5648. https://doi.org/10.1074/jbc.RA117.000596.
59. Casler, J.C., Harper, C.S., White, A.J., Anderson, H.L., and Lackner, L.L. (2024). Mitochondria-ER-PM contacts regulate mitochondrial division and PI(4)P distribution. J. Cell Biol. *223*, e202308144. https://doi.org/10.1083/jcb.202308144.
60. Richard, M., Boulin, T., Robert, V.J.P., Richmond, J.E., and Bessereau, J.L. (2013). Biosynthesis of ionotropic acetylcholine receptors requires the evolutionarily conserved ER membrane complex. Proc. Natl. Acad. Sci. USA *110*, E1055–E1063. https://doi.org/10.1073/pnas.1216154110.
61. Lewis, S.C., Uchiyama, L.F., and Nunnari, J. (2016). ER-mitochondria contacts couple mtDNA synthesis with mitochondrial division in human cells. Science *353*, aaf5549. https://doi.org/10.1126/science.aaf5549.
62. Lin, M.T., and Beal, M.F. (2006). Mitochondrial dysfunction and oxidative stress in neurodegenerative diseases. Nature *443*, 787–795. https://doi.org/10.1038/nature05292.

63. Balch, W.E., Morimoto, R.I., Dillin, A., and Kelly, J.W. (2008). Adapting proteostasis for disease intervention. Science *319*, 916–919. https://doi.org/10.1126/science.1141448.

64. Hartl, F.U., Bracher, A., and Hayer-Hartl, M. (2011). Molecular chaperones in protein folding and proteostasis. Nature *475*, 324–332. https://doi.org/10.1038/nature10317.

65. Schapira, A.H.V. (2012). Mitochondrial diseases. Lancet *379*, 1825–1834. https://doi.org/10.1016/S0140-6736(11)61305-6.

66. Izbicka, E., and Streeper, R.T. (2021). Adaptive Membrane Fluidity Modulation: A Feedback Regulated Homeostatic System Hiding in Plain Sight. In Vivo (Athens) *35*, 2991–3000. https://doi.org/10.21873/invivo.12594.

67. Moreno, S., Klar, A., and Nurse, P. (1991). Molecular genetic analysis of fission yeast Schizosaccharomyces pombe. Methods Enzymol. *194*, 795–823. https://doi.org/10.1016/0076-6879(91)94059-l.

68. Bahler, J., Wu, J.Q., Longtine, M.S., Shah, N.G., McKenzie, A., 3rd, Steever, A.B., Wach, A., Philippsen, P., and Pringle, J.R. (1998). Heterologous modules for efficient and versatile PCR-based gene targeting in Schizosaccharomyces pombe. Yeast *14*, 943–951. https://doi.org/10.1002/(SICI)1097-0061(199807)14:10<943::AID-YEA292>3.0.CO;2-Y.

69. Hoyos-Manchado, R., Reyes-Martín, F., Rallis, C., Gamero-Estévez, E., Rodríguez-Gómez, P., Quintero-Blanco, J., Bähler, J., Jiménez, J., and Tallada, V.A. (2017). RNA metabolism is the primary target of formamide in vivo. Sci. Rep. *7*, 15895. https://doi.org/10.1038/s41598-017-16291-8.

70. Schneider, C.A., Rasband, W.S., and Eliceiri, K.W. (2012). NIH Image to ImageJ: 25 years of image analysis. Nat. Methods *9*, 671–675. https://doi.org/10.1038/nmeth.2089.

71. Markgraf, D.F., Klemm, R.W., Junker, M., Hannibal-Bach, H.K., Ejsing, C.S., and Rapoport, T.A. (2014). An ER protein functionally couples neutral lipid metabolism on lipid droplets to membrane lipid synthesis in the ER. Cell Rep. *6*, 44–55. https://doi.org/10.1016/j.celrep.2013.11.046.

72. Redón, M., Guillamón, J.M., Mas, A., and Rozès, N. (2009). Effect of lipid supplementation upon Saccharomyces cerevisiae lipid composition and fermentation performance at low temperature. Eur. Food Res. Technol. *228*, 833–840. https://doi.org/10.1007/s00217-008-0996-6.

73. Lowry, R.R. (1968). Ferric chloride spray detector for cholesterol and cholesteryl esters on thin-layer chromatograms. J. Lipid Res. *9*, 397. https://doi.org/10.1016/s0022-2275(20)43112-8.

STAR★METHODS

KEY RESOURCES TABLE

REAGENT or RESOURCE	SOURCE	IDENTIFIER
Chemicals, peptides, and recombinant proteins		
Glicina max lectin	Sigma	L1395
Nystatin	Sigma	N6261
Ketoconazole	Sigma	420600
N-acetyl-L-cysteine	Sigma	A9165
Tween 20	Sigma	P1379
Linoleic Acid	Sigma	L1376
Sorbitol	PanReac	A4992
Ethanol	PanReac	131086
PEG 4000	VWR	26606
SDS	Sigma	L3771
Triton X-100	Sigma	X100
Nonidet P40	USB	19628
MitoTracker CMxRos	ThermoFisher	M7512
Hoechst	Sigma	63493
Cycloheximide	Sigma	C7698
Ergosterol	Sigma	E6510
DAPI	Sigma	D9542
H_2DCFDA	Sigma	D6883
Experimental models: Organisms/strains		
S. pombe wild type strain 972 h$^-$Other *S. pombe* strains, see Table S1.	Laboratory stock	VA1
Oligonucleotides		
Oligonucleotides used in this study can be found in Table S2.	N/A	N/A
Recombinant DNA		
pFA6a-GFP(S65T)-kanMX6	J. Bähler	pFA6a-GFP(S65T)-kanMX6
pFA6a- kanMX6	J. Bähler	pFA6a- kanMX6
pACT1-mCherry-D4H	Martin S.	pSM2056
Software and algorithms		
ImageJ	Schneider et al. 2012	https://imagej.net/software/fiji/
Graphpad Prism 9.0	Graphpad Software	https://www.graphpad.com
Other		
μ-Slide 8 well	Ibidi	Cat#: 80826
FCS2 chamber	Bioptechs	Cat#: 060319-2-03

EXPERIMENTAL MODEL AND STUDY PARTICIPANT DETAILS

S. pombe strains and culture

S. pombe strains used in this study are listed in Table S1. Standard fission yeast growth media and molecular biology techniques were employed throughout the experiments as described in Moreno et al.[67] Sporulation agar (SPA) was used for mating and sporulation. Tetrad pulling for segregation analyses was performed in a Singer MSM 400 automated dissection microscope (Singer Instruments). For spot tests, cells were cultured mid-log phase in Edinburgh Minimal Media 2 (EMM2) media. Cell number/mL was scored in Neubauer's chamber and matched dilutions were calculated for all cultures. Serial 5-fold dilutions were plated onto solid media and incubated at the indicated temperatures. Drugs were added to both solid and liquid media in at the specified in-text indicated concentrations for sensitivity/resistance assays (nystatin, Sigma N6261; ketoconazole, Sigma 420600; N-acetyl-L-cysteine,

Sigma A9165; Tween 20, Sigma P1379). When growing at restrictive temperatures, cells were incubated in a water bath at 20°C for 6 h unless stated otherwise.

For the fluidization viability spot test (Figure 6A), three concentrations were used for each compound, the indicated, half and double. Linoleic Acid (0.5mM, Sigma L1376), Sorbitol (1.5M, PanReac A4992), Ethanol (6% v/v, PanReac 131086), PEG 4000 (5% wt/v, VWR 26606), Tween 20 (0.02% v/v, Sigma P1379) SDS (0.02% v/v, Sigma L3771), Triton X-100 (0.02% v/v, Sigma X100) and Nonidet P40 (0.02% v/v, USB 19628). All compounds were added to plates of rich media (YES). Curated data from *S. pombe* genes were obtained from Pombase.[11]

METHOD DETAILS

Gene tagging and genetics analysis

Gene tagging was performed according to described protocols,[68] using the pF6aMX6 plasmid series. Following transformation, PCR from target loci was employed to verify the integration of the tags at the expected genomic locations in the candidate strains (the list of oligonucleotides used in this study can be found in Table S2). Tetrad analysis for single integrations and double mutant's constructs was performed by tetrads dissection following described methods.[67] Strains used in this study are listed in the STAR Methods section.

Fluorescence microscopy

For live-cell imaging, cells were mounted in an Ibidi μ-Slide 8 Well chamber (Ibidi 80826) adhered to the chamber with soybean lectin (Sigma L1395). (Cells were kept alive in EMM2). Imaging was conducted using a spinning-disk confocal microscope (IX-81, Olympus; CoolSNAP HQ2 camera, Plan Apochromat 100x, 1.4 NA objective, Roper Scientific) and Metamorph software, with the temperature maintained at 20 or 30°C.

For DAPI/Calcofluor Staining, we followed the protocol described in Hoyos-Manchado et al.[69] Images were captured using a Nikon ECLIPSE Ti-S microscope equipped with a Plan Apo VC 60x/1.40 Oil NA lens.

All images were processed using the open-source software ImageJ (Fiji).[70] Unless otherwise stated in the figure legend, the images presented in the figures correspond to maximal projections of 26 slices with a Z-step of 0.3 μm.

For MitoTracker-Hoechst staining in *S. pombe* cultures, cells were cultured in minimal medium until reaching an exponential phase of $2x10^6$cell/mL. MitoTracker CMxRos (200 nM in medium from the stock of 1 mM in DMSO, ThermoFisher M7512) and Hoechst (0.5–1 μg/mL in water from stock stored at 4°C, Sigma 63493) solutions were used for staining the cells.

Fluorescence Recovery After Photo bleaching (FRAP) was performed using a spinning-disk confocal microscope (IX-81, Olympus; CoolSNAP HQ2 camera, Plan Apochromat 100x, 1.4 NA objective, Roper Scientific) and Metamorph software. A region of the cell was targeted, and recovery of the fluorescence was measured. Cells were incubated 30 min with cycloheximide (150 μm/mL, Sigma C7698) prior imaging.

mtDNA qPCR

To extract mitochondrial DNA (mtDNA) from *S. pombe*, cells were cultured in rich medium (YES) until exponential phase (about $2x10^6$ cell/mL) at the desired temperature (20 or 30°C). Extract DNA from cultures using a FastPrep-24 5G (Fisher Scientific) machine and later purification by phenol-chloroform. DNA concentrations were measured using a NanoDrop 2000 (Thermo Fisher Scientific) and adjusted to 20 ng/μL. Sample integrity was verified using a simple PCR with one of the qPCR primers. To perform the qPCR, 20 ng of DNA from the samples was added per triplicate, along with SYBR Green (Takara Bio RR820L) following the manufacturer's instructions and 1 μL of each primer (Table S2) diluted to 100 nM. The qPCR was carried out with the following parameters: 1x 95°C for 3′ and 40x 95°C for 10'' + 62°C for 30″, followed by a melting curve from 62°C to 95°C. The $2^{-\Delta Ct}$ and $2^{\Delta\Delta Ct}$ were calculated and the obtained data were normalized with respect to the *wild-type*.

TLC of ergosterol

Lipids were extracted from cells following the protocol by Markgraf et al.[71] Briefly, cells were cultured until the exponential phase. Cells were collected and resuspended in 330 μL of methanol with glass beads and pulsed in a fast-prep. Then 660 μL of chloroform were added, centrifuged and the supernatant was recovered and 0.2 volumes of 0.9% NaCl were added. After the formation of two phases, the lower phase was recovered and evaporated completely using a SpeedVac. The residue was resuspended in 20 μL of chloroform. To perform lipid separation, TLC silica gel 60 F_{254} plates of 10 × 20 cm were prepared, and samples of known concentrations (0.25, 0.5, and 1 mg/mL) of ergosterol (sigma E6510) were prepared. 10 μL of each sample and of the ergosterol solutions were deposited, leaving at least 1 cm of separation between them. The separation was performed in three phases following described protocols[72] In summary, a first stage up to 50% of the maximum migration with hexane:diethyl ether:glacial acetic acid (50:50:2), a second stage up to 80% of the maximum migration with hexane:diethyl ether:glacial acetic acid (80:20:2), and finally a third stage to the maximum migration with 100% hexane. To reveal the lipids once separated, a ferric chloride solution (50 mg of $FeCl_3 \cdot 6H_2O$ in 90 mL of water) with 5 mL of glacial acetic acid and 5 mL of concentrated H_2SO_4 is sprayed over the TLC plate and heated at 100°C for 3 min.[73] Plates were scanned using a GelDoc Go (BioRad 12009077) system and quantified in ImageJ software using the standard curve of pure ergosterol.

QUANTIFICATION AND STATISTICAL ANALYSIS

Quantification of fluorescent signals

The fluorescence intensity in Figures 4B, 6A, and S1A was measured by defining a region of interest around the targeted area and subtracting fluorescence within an equivalent background area. To analyze fluorescence intensity dynamics in Figures 5D and 5A region of interest was traced and the average intensity per pixel was calculated while subtracting the background over time. To maintain consistency, the fluorescence images of both the wild-type and mutant samples were acquired simultaneously.

Statistical analysis

Graphs and statistical analyses were produced using Microsoft Excel and Prism 9.4.1 (GraphPad Software). The number of cells analyzed (n) is defined in each Figure and were derived from at least three independent experiments. The graphs display the mean and the error bars correspond to the standard deviation (SD) between experiments as specifically indicated in each Figure. For comparisons between two groups in Figures 2B and 5F, an unpaired Student's test was used. Paired Student's test was used in Figure 5D. Multiple-group comparisons were conducted in Figures 4A, 4B, 5C, 6A, and S1B using non-parametric ordinary one-way ANOVA. Statistical significance was considered for p values lower than 0.05(*). p values exceeding 0.05 were considered to be ns (non-significant). Further details of statistical analysis are given in the figure legends.